atoms

IMPACT FACTOR 1.5

CITESCORE 3.1

Article

# *g*-Factor Isotopic Shifts: Theoretical Limits on New Physics Search

Dmitry S. Akulov, Rinat R. Abdullin, Dmitry V. Chubukov, Dmitry A. Glazov and Andrey V. Volotka

MDPI

https://doi.org/10.3390/atoms13060052

atoms

MDPI

*Article*

# *g*-Factor Isotopic Shifts: Theoretical Limits on New Physics Search

**Dmitry S. Akulov, Rinat R. Abdullin, Dmitry V. Chubukov *, Dmitry A. Glazov and Andrey V. Volotka**

School of Physics and Engineering, ITMO University, Kronverkskiy 49, St. Petersburg 197101, Russia; dmitriy.akulov@metalab.ifmo.ru (D.S.A.); rinat.abdullin@metalab.ifmo.ru (R.R.A.); dmitry.glazov@metalab.ifmo.ru (D.A.G.); andrey.volotka@metalab.ifmo.ru (A.V.V.)
* Correspondence: dmitry.chubukov@metalab.ifmo.ru

**Abstract:** The isotopic shift of the bound-electron $g$ factor in highly charged ions (HCI) provides a sensitive probe for testing physics beyond the Standard Model, particularly through interactions mediated by a hypothetical scalar boson. In this study, we analyze the sensitivity of this method within the Higgs portal framework, focusing on the uncertainties introduced by quantum electrodynamics corrections, including finite nuclear size, nuclear recoil, and nuclear polarization effects. All calculations are performed for the ground-state $1s$ configuration of hydrogen-like HCI, where theoretical predictions are most accurate. Using selected isotope pairs (e.g., $He^{4/6}$, $Ne^{20/22}$, $Ca^{40/48}$, $Sn^{120/132}$, $Th^{230/232}$), we demonstrate that the dominant source of uncertainty arises from finite nuclear size corrections, which currently limit the precision of new physics searches. Our results indicate that the sensitivity of this method decreases with increasing atomic number. These findings highlight the necessity of improved nuclear radius measurements and the development of alternative approaches, such as the special differences method, to enable virtually the detection of fifth-force interactions.

**Keywords:** quantum electrodynamics; bound-electron $g$ factor; fifth-force search; Higgs portal model; finite nuclear size corrections; isotopic shift



Academic Editor: Kanti M. Aggarwal

Received: 26 April 2025
Revised: 5 June 2025
Accepted: 11 June 2025
Published: 13 June 2025

**Citation:** Akulov, D.S.; Abdullin, R.R.; Chubukov, D.V.; Glazov, D.A.; Volotka, A.V. *g*-Factor Isotopic Shifts: Theoretical Limits on New Physics Search. *Atoms* **2025**, *13*, 52. https://doi.org/10.3390/atoms13060052



## 1. Introduction

The $g$ factor of an electron is one of the key quantities in quantum electrodynamics (QED), expressing the relationship between the magnetic moment of an electron and its spin. For many years, the free-electron $g$ factor has served as a high-precision test of QED and, in a broader context, the Standard Model (SM) of electroweak interactions [1,2]. In this regard, bound electron provides access to the relativistic domain, where the nontrivial effects are enhanced by the strong field of the nucleus. Recent measurements in highly charged ions have achieved a relative accuracy of a part in $10^{12}$ (see Refs. [3–7] and the references therein) and continue to improve [8–11]. The accuracy of theoretical calculations also increases [12,13] as higher-order corrections are taken into account, such as nuclear polarization [14–17], nuclear deformation [18,19], higher-order nuclear recoil, finite nuclear size effects [20], and others.

At the same time, an increasing number of extensions beyond the SM, referred to as new physics, aim to address several fundamental problems, including the nature of dark matter and dark energy [21], the electroweak hierarchy problem [22], and baryon asymmetry [23]. Among various high-precision atomic physics techniques, high-resolution isotope shift spectroscopy of the $g$ factor of a bound electron has emerged as a sensitive method to probe such new physics scenarios (see Refs. [24,25] and the references therein).

The corresponding measurements have been accomplished recently in Refs. [7,11] to confirm in particular the theory of the relativistic nuclear recoil effect [26–28].

In this paper, we focus on the isotopic shift of the bound-electron $g$ factor in hydrogen-like highly charged ions (HCIs), restricting our analysis to the ground $1s$ state, where both experimental and theoretical uncertainties are minimal. The isotopic shift is defined as the difference in the $g$ factors of two isotopes $A$ and $A'$ of a given element:

$$g^{AA'} = g^{A} - g^{A'}. \tag{1}$$

In the leading orders of expansion in the electron-to-nucleus mass ratio $\frac{m}{M}$ and the mean-square nuclear radii $\langle r^2 \rangle$, the isotopic shift can be represented as

$$g^{AA'} = g^{AA'}_{\mathrm{FS}} + g^{AA'}_{\mathrm{NP}} + g^{AA'}_{\mathrm{MS}} + g^{AA'}_{\mathrm{NB}}, \tag{2}$$

where $g^{AA'}_{\mathrm{FS}}$ denotes the field shift contribution, which originates from the difference in the mean-square nuclear charge radii of two isotopes, the term $g^{AA'}_{\mathrm{NP}}$ corresponds to nuclear polarization correction and despite of relative smallness of its value, its contribution into isotope shift can be of comparable magnitude with finite nucleus and recoil contributions, the term $g^{AA'}_{\mathrm{MS}}$ represents the mass shift contribution, arising from the difference in nuclear masses, $(M_A - M_{A'})$, and finally, $g^{AA'}_{\mathrm{NB}}$ accounts for a possible contribution from spin-independent interactions between the bound electron and the nucleus, such as those mediated by hypothetical scalar bosons.

Each of the terms in Equation (2) is affected by different sources of uncertainty. Some uncertainties, such as those related to nuclear models or experimental values of nuclear charge radii, are currently difficult to reduce. Others, such as higher-order recoil or radiative corrections, are primarily theoretical in nature and can, in principle, be improved with further refinements.

In this paper, we analyze the influence of all these effects on the sensitivity of the isotope shift method in the search for new physics, using a selection of isotope pairs. Our paper is organized as follows. In Section 2, we outline the model of a hypothetical fifth force used and the essence of the testing method. In Sections 3 and 4, we discuss the influence of various corrections. In Section 5, we analyze the sensitivity of this method for various isotopes and present several graphs of the new physics constant as a function of the boson mass. In Section 6, we draw a conclusion.

Throughout the text, we employ relativistic units $\hbar = c = 1$, $\alpha = e^2/(4\pi) \approx 1/137$ (where $\hbar$ is the Planck constant, $c$ is the speed of light, $\alpha$ is the fine-structure constant, and $e$ is the elementary charge).

## 2. Fifth-Force Model

There are many candidates for a hypothetical fifth interaction and various methods for its detection (see Ref. [29] and the references therein). In this study, we employ the Higgs portal model [29] as a model for the fifth force. This model describes the spin-independent interaction between nucleons and electrons. Scalar bosons associated with this interaction may provide solutions to the long-standing electroweak hierarchy problem and are considered promising candidates to address the dark matter problem. The potential exerted on the electrons by this force is of Yukawa type:

$$V_\phi(r) = -\alpha_{\mathrm{NB}} A \frac{e^{-m_\phi r}}{r}, \tag{3}$$

where $m_\phi$ denotes the mass of the boson and $\alpha_{\mathrm{NB}} = \frac{y_e y_n}{4\pi}$ represents the coupling constant

of new physics, where $y_e$ and $y_n$ are the couplings of the scalar boson to electrons and nucleons, respectively, and $A$ is the atomic number.

The result of the interaction described by the Feynman diagram depicted in Figure 1 is expressed by the following matrix element:

$$g_{\mathrm{NB}}^{AA'} = \frac{< i|[\boldsymbol{\alpha} \times \boldsymbol{r}]_z|n >< n|V_\phi|i >}{E_i - E_n}, \tag{4}$$

where $|i\rangle$ ($|n\rangle$) and $E_i$ ($E_n$) denote the initial (intermediate) electronic state and the corresponding energy, respectively, the vector $\boldsymbol{\alpha}$ represents the Dirac matrices, and $[\boldsymbol{\alpha} \times \boldsymbol{r}]_z$ corresponds to the $z$-component of the relativistic magnetic moment operator. Following Refs. [24,25], the new-physics contribution to the isotopic $g$-factor shift (i.e., the difference in the $g$ factor between isotopes with mass numbers $A$ and $A'$) can be expressed in closed form as

$$g_{\mathrm{NB}}^{AA'} = -\frac{4}{3}\alpha_{\mathrm{NB}}\frac{(Z\alpha)}{\gamma}\,(A - A')\left(1 + \frac{m_\phi}{2Z\alpha m}\right)^{-2\gamma}\left[3 - 2\frac{(Z\alpha)^2}{1+\gamma} - \frac{2\gamma}{1 + \frac{m_\phi}{2Z\alpha m}}\right]. \tag{5}$$

The expression for $g_{\mathrm{NB}}^{AA'}$ describes the leading-order correction to the $g$ factor of an electron in the $1s$ state due to the exchange of a massive scalar boson $\phi$ between the electron and the nucleus. The parameter $\gamma = \sqrt{\kappa^2 - (Z\alpha)^2}$ incorporates relativistic effects, with $\kappa$ being the relativistic angular quantum number, $Z$ the nuclear charge, and $m$ the electron mass.

**Figure 1.** Feynman diagram corresponding to the leading order contribution of new physics to the $g$ factor of a bound electron. The double line represents the bound electron, the wavy line terminated by a triangle represents interaction with an external magnetic field, and the dashed line terminated by a rhombus denotes the electron–nucleus interaction via exchange by a scalar boson.

In the mass range considered in this work, the finite nuclear size (FNS) effects are strongly suppressed, and therefore, neglected in Equation (5). The heaviest bosons included in our analysis correspond to interaction ranges that are several times larger than a typical nuclear radius. As a result, the boson-mediated interaction effectively probes the nucleus as if it were point-like. This makes the nuclear size effects insignificant for the entire parameter space explored in this study.

To quantify the strength of a hypothetical new interaction, we relate the observed uncertainty $\Delta g^{AA'}$ to the theoretically predicted shift $g_{\mathrm{NB}}^{AA'}$ induced by the exchange of a new boson. In this context, we express the effective coupling constant of the new interaction as the ratio between the observed deviation and the model prediction for the boson-mediated shift.

The present paper examines the uncertainties associated with these contributions and their impact on the sensitivity of the isotopic shift method by analyzing multiple isotope pairs. The selected pairs include $\mathrm{He}^{4/6}$, $\mathrm{Ca}^{40/42}$, $\mathrm{Ca}^{40/48}$, $\mathrm{Sn}^{120/132}$, and $\mathrm{Th}^{230/232}$. For calcium, two distinct pairs were chosen: $\mathrm{Ca}^{40/42}$ to enable direct comparison with prior studies and $\mathrm{Ca}^{40/48}$ due to its experimental feasibility.

In subsequent sections, we examine the QED corrections and their uncertainties. The corrections are categorized into two sections: purely theoretical corrections, in which accuracy can be improved (mass shift), and corrections, in which accuracy is limited by experiment (field shift).

## 3. Nuclear Size and Polarization Effects

A pair of isotopes differs in mass and nuclear charge distribution. The latter fact leads to the difference in nuclear potential. The shift of the $g$ factor related to the difference in nuclear potentials is known as the field shift (FS). In the present work, it is assumed that all isotopes have the same charge distribution profile: the two-parameter Fermi distribution. In the present approach, all the parameters of the distribution are the same except the nuclear charge radii. Thus, $g_{\rm FS}^{AA'}$ can be expressed as follows:

$$g_{\rm FS}^{AA'} = g^{A} - g^{A'}. \tag{6}$$

In the present work, $g$ factor values are calculated numerically by solving the Dirac equation with arbitrary potential $V$ within a dual kinetic balance approach [30].

### *3.1. Radii Uncertainty*

Data on atomic radii and their uncertainties and errors of the differences of atomic radii of isotope pairs are taken from [31,32].

Let us consider the total uncertainty in the calculation of $\Delta g$ due to isotope radius uncertainty as

$$\Delta g_{R}^{AA'} = \sqrt{\Delta g_{R_1}^2 + \Delta g_{R_2}^2 + \Delta g_{R_3}^2} \tag{7}$$

to take into account correlations in radii uncertainties.

$$\Delta g_{R_1} = \left(g_{R}^{A} - g_{R'}^{A'}\right) - \left(g_{R+\delta R}^{A} - g_{R'+\delta R}^{A'}\right), \tag{8}$$

$$\Delta g_{R_2} = \left(g_{R}^{A} - g_{R'}^{A'}\right) - \left(g_{R+\delta R'}^{A} - g_{R'+\delta R'}^{A'}\right), \tag{9}$$

$$\Delta g_{R_3} = \left(g_{R}^{A} - g_{R'}^{A'}\right) - \left(g_{R}^{A} - g_{R'+\delta(RR')}^{A'}\right). \tag{10}$$

The term $\left(g_{R}^{A} - g_{R'}^{A'}\right)$ in Equations (8)–(10) provides contribution into isotope shift associated with the isotope radius difference. The next expression in brackets in Equation (8) gives the contribution into uncertainty of $\Delta g_R$ caused by the error in the radius of isotope $A$ definition. Similarly, the expression (9) is defined. It involves an error that arises from the uncertainty in the determination of the radius $R'$. Also, in Equations (8)–(10), $\delta R$ and $\delta R'$ denote uncertainties of the radii of isotopes $A$ and $A'$, respectively. In Equation (10), $\delta(RR')$ is the difference of $\delta R$ and $\delta R'$ uncertainties.

Equation (10) accounts for the asymmetry in the uncertainties of the radii of the two isotopes when $\delta R \neq \delta R'$. This is important because if one radius is measured with higher precision, the contribution to the g-factor difference may be underestimated unless this discrepancy is explicitly considered. In essence, $\Delta g_{R_3} \approx \left(\partial g^{A'}/\partial R'\right) \cdot \delta R'$, where $\delta R$ denotes the uncertainty in the radius of the other isotope. This term, thus, represents a correction for incomplete error compensation when the uncertainties "differ" in magnitude. This approach is equivalent to analyzing the limiting case in which one radius is overestimated while the other is underestimated, thereby yielding the maximum spread in the isotope shift [33].

The contributions of these uncertainties to the isotope shift of the $g$ factor are summarized in Table 1. From Table 1, it follows that the $\Delta g$ values for the pair of isotopes $Ca^{40/42}$ are three orders of magnitude greater than those for the pair $Ca^{40/48}$. This discrepancy can be attributed to the fact that the field shift is proportional to the radius difference. Despite the larger difference in mass numbers, the radius difference is greater for the $Ca^{40/42}$ isotopes [31,32].

The other way to obtain the total uncertainty is to consider the maximum deviation of $R$ and to estimate $\Delta g_R$ as the square root of the sum of squared differences originating from the maximum variation of the radii. This approach does not take into account possible correlations and leads to a larger value of uncertainty. At least, this method allows us to obtain an upper bound on the uncertainty. These contributions are presented in the Table 2.

$$\Delta g_R = \sqrt{(g^A_{R+\delta R} - g^A_{R-\delta R})^2 + (g^{A'}_{R+\delta R} - g^{A'}_{R-\delta R})^2}. \tag{11}$$

**Table 1.** Uncertainties arising from errors in radius values, taking into account correlations between uncertainties. $\Delta g$ values should be multiplied by $10^{-9}$.

| Contribution | $^{4/6}$He | $^{20/22}$Ne | $^{40/42}$Ca | $^{40/48}$Ca | $^{120/132}$Sn | $^{230/232}$Th |
|---|---|---|---|---|---|---|
| $\Delta g^{AA'}_{R_1}$ | $4.55 \times 10^{-4}$ | $7.3 \times 10^{-5}$ | $-0.019$ | $-1.9 \times 10^{-5}$ | 0.224 | $-181$ |
| $\Delta g^{AA'}_{R_2}$ | $4.71 \times 10^{-4}$ | $-2.19 \times 10^{-4}$ | $-0.019$ | $-2.5 \times 10^{-5}$ | 2.57 | 4.84 |
| $\Delta g^{AA'}_{R_3}$ | $4.9 \times 10^{-4}$ | $-2.19 \times 10^{-4}$ | $-0.02$ | $7 \times 10^{-6}$ | 1.78 | $-0.258$ |
| $\Delta g^{AA'}_{R\ \text{total}}$ | $8.15 \times 10^{-4}$ | $2.59 \times 10^{-4}$ | 0.033 | $3.21 \times 10^{-5}$ | 3.85 | 181 |

**Table 2.** Uncertainties arising from errors in radius values without corellations. The $\Delta g$ value should be multiplied by $10^{-9}$.

| Contribution | $^{4/6}$He | $^{20/22}$Ne | $^{40/42}$Ca | $^{40/48}$Ca | $^{120/132}$Sn | $^{230/232}$Th |
|---|---|---|---|---|---|---|
| $\Delta g^{AA'}_{R\ \text{total}}$ | 0.017 | 0.03 | 1.53 | 1.55 | 92.41 | 9560 |

### *3.2. Nuclear Model Uncertainty*

As a nuclear model, the two-parameter Fermi nuclear charge distribution is considered:

$$\rho(r) = \frac{\rho_0}{1 + \exp\left(\frac{r-c}{a}\right)}. \tag{12}$$

The $\rho_0$ should be obtained with the normalization condition

$$4\pi \int \rho(r) r^2 dr = 1. \tag{13}$$

The parameter $a = t/4\ln 3$, $t = 2.3$ matches all isotopes. This value reproduces measured charge radii, isotopic shifts, and hyperfine structure data across multiple nuclei [31,32]. The value $t = 2.3$ fm is a robust compromise validated by both experimental and theoretical studies, capturing the universal surface properties of heavy nuclei while minimizing computational complexity. For light nuclei, the Fermi distribution is often a poor approximation. Although $t \simeq 1.0 - 2.0$ fm can be applied for $A \geq 6$, cluster or ab initio densities are preferred for greater precision. The default value for heavy nuclei ($t \simeq 2.3$ fm) is inadequate in this context due to fundamentally different nuclear structures [34–36]. We chose to adjust the parameter $t$ proportionally and take the following values: $t = 1.15$ fm for neon isotopes and $t = 0.575$ fm for helium isotopes.

The uncertainty related to the choice of nuclear model is established by varying the coefficient $a$, which is responsible for the skin thickness of the distribution. Thus, the error of the model is defined as

$$\Delta g_{\text{model}} = \sqrt{\left[g^A_{\text{fns}}(a) - g^A_{\text{fns}}(a/2)\right]^2 + \left[g^{A'}_{\text{fns}}(a) - g^{A'}_{\text{fns}}(a/2)\right]^2}, \tag{14}$$

where $g^{A'}_{\text{fns}}(a)$ is a finite correction of nuclear size to the $g$ factor of the isotope $A'$ with the $a$ value of the Fermi model parameter. Since at the moment there is no exact knowledge of

the nuclear model, this error is irrecoverable. Total model uncertainty contribution into isotope shift is summarized in the Table 3.

**Table 3.** Uncertainties arising from the model. The $\Delta g$ value should be multiplied by $10^{-9}$.

| Contribution | $He^{4/6}$ | $Ne^{20/22}$ | $Ca^{40/42}$ | $Ca^{40/48}$ | $Sn^{120/132}$ | $Th^{230/232}$ |
|---|---|---|---|---|---|---|
| $\Delta g^{AA'}_{\text{model}}$ | $2.16 \times 10^{-5}$ | $1.1 \times 10^{-3}$ | $5.63 \times 10^{-2}$ | $5.64 \times 10^{-2}$ | 19.9 | 2180 |

### *3.3. Nuclear Polarization*

The phenomenon of nuclear polarization originates from the interaction between the nucleus and electrons through real or virtual electromagnetic excitations. This phenomenon leads to a contribution of nuclear polarization (NP) to the binding energy and the $g$ factor of the bound electron [14]. The treatment of nuclear polarization within the QED framework was developed in Ref. [15]. This approach is approximate, and due to the phenomenological description of the nucleon–nucleon interaction, nuclear polarization correction set the ultimate accuracy limit up to which the QED corrections can be tested in highly charged ions. Contributions from low-lying nuclear states were obtained using experimental values for nuclear excitation energies $w_L$ and reduced electric transition probabilities [16]. Contributions upcoming from giant resonances were calculated with employing empirical sum rules [17]. In the present calculations, contributions due to monopole, dipole, quadrupole, and octupole giant resonances have been taken into account. To evaluate the infinite summations over the entire Dirac spectrum, the finite basis set method has been employed [37].

In this paper, we define the uncertainty of the nuclear polarization contribution to the $g$ factor isotope shift as 50% of its value.

### *3.4. Field Shift Correction and Uncertainties*

Values of finite nuclear size and nuclear polarization corrections are presented in Table 4.

**Table 4.** Field shift and nuclear polarization contributions into isotope shifts. All values should be multiplied by $10^{-9}$.

| Contribution | $He^{4/6}$ | $Ne^{20/22}$ | $Ca^{40/42}$ | $Ca^{40/48}$ | $Sn^{120/132}$ | $Th^{230/232}$ |
|---|---|---|---|---|---|---|
| FNS | $-7.5 \times 10^{-4}$ | 0.17 | $-1.99$ | $3.2 \times 10^{-3}$ | $-332$ | $-4720$ |
| NP | $\leq 10^{-6}$ | $5 \times 10^{-5}$ | $1.73 \times 10^{-2}$ | $7.8 \times 10^{-3}$ | $-0.136$ | 59.3 |

The main contribution to the uncertainty of the $g$ factor arises from the error in the value of the root mean square charge radius. This error is mainly determined by the experimental accuracy. Individual contributions to the final result can be found in the Table 5.

**Table 5.** Main uncertainties in the field shift and nuclear polarization contributions to isotope shifts for selected elements. $\Delta g$ values should be multiplied by $10^{-9}$.

| Contribution | $He^{4/6}$ | $Ne^{20/22}$ | $Ca^{40/42}$ | $Ca^{40/48}$ | $Sn^{120/132}$ | $Th^{230/232}$ |
|---|---|---|---|---|---|---|
| $\Delta g^{AA'}_{\text{nucl.pol}}$ | $\leq 0.0001$ | $\leq 0.0001$ | 0.008 | 0.004 | 0.068 | 29.64 |
| $\Delta g^{AA'}_{R}$ | $8.15 \times 10^{-4}$ | $2.59 \times 10^{-4}$ | 0.033 | $3.21 \times 10^{-5}$ | 3.85 | 181 |
| $\Delta g^{AA'}_{\text{model}}$ | $2.16 \times 10^{-5}$ | $1.1 \times 10^{-3}$ | $5.63 \times 10^{-2}$ | $5.64 \times 10^{-2}$ | 19.9 | 2180 |

## 4. Nuclear Recoil Effect

Mass shift corrections include contributions from nuclear recoil processes, which are limited by theoretical accuracy. In the evaluation of corrections to the bound-electron $g$ factor, the nuclear recoil effect plays a significant role. For $ns$ states in the nonrelativistic limit, this contribution vanishes due to the specific kinematics of the electron–nucleus system. However, relativistic effects lead to a nonzero correction, primarily determined by the electron-to-nucleus mass ratio $m/M$ and the parameters $\alpha Z$ and $\alpha$. When studying relativistic corrections arising from nuclear recoil in high-$Z$ ions, it is essential to derive an exact analytical expression that accounts for the $\alpha Z$ dependence to the first order in the mass ratio $m/M$. This solution was originally derived in Ref. [38]. An analytical calculation of the lower-order $\alpha Z$ correction yields an expression derived within the framework of the point-nucleus approximation:

$$g_{\mathrm{L}}^{AA'} = m\left(\frac{1}{M} - \frac{1}{M'}\right)\left[(\alpha Z)^2 - \frac{(\alpha Z)^4}{3\left(1+\sqrt{1-(\alpha Z)^2}\right)^2}\right]. \tag{15}$$

The first term represents the leading contribution, while the second term starts to contribute from order $(\alpha Z)^4$ and higher. In this work, we calculate it for a finite nucleus. Thus, the leading source of error in this contribution is the finite nuclear size uncertainty. The uncertainty in the final nuclear size correction is determined by both the model uncertainty and the radius uncertainty:

$$\Delta g_{\mathrm{L}}^{AA'} = \Delta g_{\mathrm{recmodel}_L}^{AA'} + \Delta g_{\mathrm{recradii}_L}^{AA'}. \tag{16}$$

In particular, the model uncertainty is quantified as

$$\Delta g_{\mathrm{recmodel}_L}^{AA'} = (g_{\mathrm{L}_a}^{A} - g_{\mathrm{L}_a}^{A'}) - (g_{\mathrm{L}_{a/2}}^{A} - g_{\mathrm{L}_{a/2}}^{A'}), \tag{17}$$

which corresponds to the difference between the results obtained using the Fermi model for the nuclear charge distribution with the Fermi parameter set to $a$ and those obtained with the parameter set to $a/2$. The radii uncertainty is estimated as

$$\Delta g_{\mathrm{recradii}_L}^{AA'} = \sqrt{(g_{\mathrm{L}_{R+dR}}^{A} - g_{\mathrm{L}_{R-dR}}^{A})^2 + (g_{\mathrm{L}_{R+dR}}^{A'} - g_{\mathrm{L}_{R-dR}}^{A'})^2}. \tag{18}$$

Assuming that these radii uncertainties are uncorrelated, they are combined in quadrature.

In addition to the lower-order correction, the higher-order contribution is significant. This contribution is given by the sum of the Coulomb and the transverse-photon exchange parts and can be written as

$$g_{\mathrm{H}}^{AA'} = m\left(\frac{1}{M} - \frac{1}{M'}\right)(\alpha Z)^5 P(\alpha Z). \tag{19}$$

For this contribution, the detailed formulas are provided in Ref. [38]. The calculations for the 1S state are presented in Ref. [28], where the function $P(\alpha Z)$ characterizes the combined effect of the corrections arising from a full relativistic treatment. We take the values for $P(\alpha Z)$ for the point-nucleus case from Ref. [28], while for the finite nucleus, representative values have been obtained from numerical calculations. The higher-order contribution is generally rather large; in particular, it exceeds the $(\alpha Z)^4(m/M)$ term of Equation (16) even for $Z = 1$. Nevertheless, for all elements except thorium, $g_{\mathrm{H}}^{AA'}$ is smaller than $g_{\mathrm{L}}^{AA'}$. The error is estimated using this simple ratio

$$\Delta g_{\mathrm{H}}^{AA'} = g_{\mathrm{H}}^{AA'} \frac{\Delta g_{\mathrm{L}}^{AA'}}{g_{\mathrm{L}}^{AA'}}. \tag{20}$$

The complete nuclear recoil correction includes not only the first-order term in $m/M$ discussed above but also known second-order corrections proportional to $(m/M)^2$ and mixed terms proportional to $\alpha(m/M)$ and $\alpha(m/M)^2$ [39–43]. The mixed terms, commonly referred to as radiative recoil corrections, account for the effects of radiation processes (such as photon emission and reabsorption) on the nuclear recoil. The $(m/M)^2$ corrections arise from higher-order recoil effects, which become increasingly important for high-$Z$ systems. These additional contributions, together with the lower-order and higher-order corrections described above, are combined with the radiative and second-order in $m/M$ recoil corrections to ensure the required accuracy for comparing theoretical predictions with high-precision experimental determinations of the $g$ factor [13].

$$g_{(m/M)^2}^{AA'} = -(\alpha Z)^2(1+Z)m^2\left(\frac{1}{M_A^2} - \frac{1}{M_{A'}^2}\right), \tag{21}$$

$$g_{\mathrm{radrecoil}}^{AA'} = \frac{\alpha}{\pi}(\alpha Z)^2\left[-\frac{1}{3}m\left(\frac{1}{M_A} - \frac{1}{M_{A'}}\right) + \frac{3-2Z}{6}m^2\left(\frac{1}{M_A^2} - \frac{1}{M_{A'}^2}\right)\right]. \tag{22}$$

We know the radiative recoil corrections and the second-order $m/M$ corrections to the recoil at the leading order in $\alpha Z$. Accordingly, the dominant uncertainty for these contributions can be estimated from the neglected higher-order terms as follows:

$$\Delta g_{(m/M)^2}^{AA'} = (\alpha Z)^2 g_{(m/M)^2}^{AA'}, \tag{23}$$

$$\Delta g_{\mathrm{radrecoil}}^{AA'} = (\alpha Z)^2 g_{\mathrm{radrecoil}}^{AA'}. \tag{24}$$

It should be noted that the uncertainty arising from the finite nuclear size (FNS) is not the leading source of error for these contributions.

The recoil effect decomposition in isotope shifts for selected elements is presented in Table 6, while the main uncertainties in the recoil contributions to isotope shifts are summarized in Table 7.

**Table 6.** Recoil effect decomposition in isotope shifts for selected elements. All values should be multiplied by $10^{-9}$.

| Contribution | $^{4/6}$He | $^{20/22}$Ne | $^{40/42}$Ca | $^{40/48}$Ca | $^{120/132}$Sn | $^{230/232}$Th |
|---|---|---|---|---|---|---|
| $(m/M)$ Non-QED | 9.780 | 13.276 | 13.882 | 48.622 | 54.49 | 7.3 |
| $(m/M)$ QED | 0.0005 | 0.0436 | 0.2598 | 0.9100 | 10.4496 | 10.939 |
| $(\alpha)(m/M)$ | −0.0076 | −0.0103 | −0.0108 | −0.0377 | −0.043 | −0.007 |
| $(m/M)^2$ | −0.0067 | −0.0077 | −0.0078 | −0.0257 | −0.025 | −0.004 |
| $g_{\mathrm{MS}}^{AA'}$ | 9.7662 | 13.3012 | 14.1232 | 49.4686 | 64.8716 | 18.228 |

**Table 7.** Main uncertainties in the recoil contributions to isotope shifts for selected elements. $\Delta g$ values should be multiplied by $10^{-9}$.

| Contribution | $^{4/6}$He | $^{20/22}$Ne | $^{40/42}$Ca | $^{40/48}$Ca | $^{120/132}$Sn | $^{230/232}$Th |
|---|---|---|---|---|---|---|
| $\Delta g_{\mathrm{L}}^{AA'}$ | ≤0.0001 | ≤0.0001 | ≤0.0001 | ≤0.0001 | 0.01 | 0.5 |
| $\Delta g_{\mathrm{H}}^{AA'}$ | ≤0.0001 | ≤0.0001 | ≤0.0001 | ≤0.0001 | 0.0002 | 0.003 |

**Table 7.** *Cont.*

| Contribution | $He^{4/6}$ | $Ne^{20/22}$ | $Ca^{40/42}$ | $Ca^{40/48}$ | $Sn^{120/132}$ | $Th^{230/232}$ |
|---|---|---|---|---|---|---|
| $\Delta g^{AA'}_{\text{radrecoil}}$ | ≤0.0001 | ≤0.0001 | 0.0002 | 0.0008 | 0.006 | 0.003 |
| $\Delta g^{AA'}_{(m/M)^2}$ | ≤0.0001 | ≤0.0001 | 0.0002 | 0.0005 | 0.003 | 0.002 |
| $\Delta g^{AA'}_{\text{MS}}$ | ≤0.0001 | ≤0.0001 | 0.0004 | 0.0013 | 0.0192 | 0.508 |

## 5. Discussion

Figures 2 and 3 show the dependence of the new physics coupling constant $\alpha_{\text{NB}}$ on the scalar boson mass $m_\phi$ for the selected isotope pairs. Our calculations reveal a systematic decrease in the sensitivity of the isotope-shift method with increasing atomic number $Z$: for heavier ions, the larger relativistic enhancements are offset by growing theoretical and experimental uncertainties.

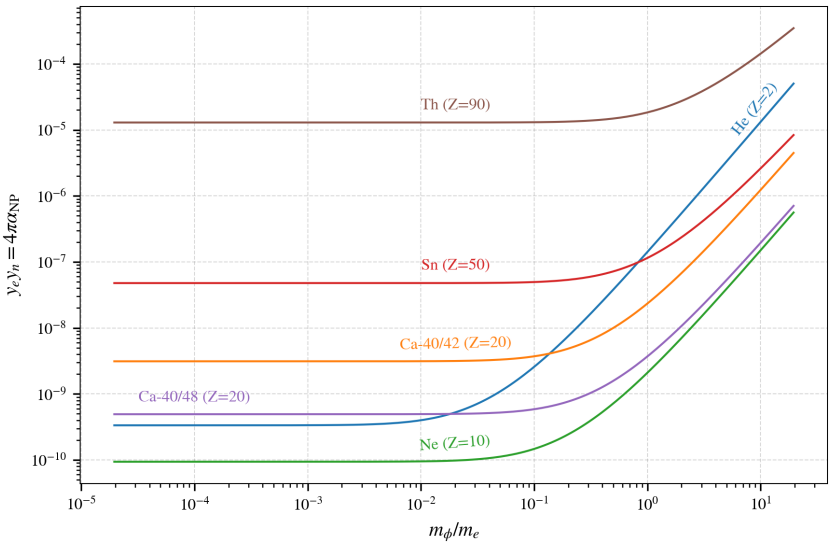


**Figure 2.** Constraints on the new physics coupling constant $\alpha_{\text{NB}}$ as a function of the scalar boson mass $m_\phi$ derived from isotope shift measurements of the bound-electron $g$ factor. Uncertainties are evaluated using the root-mean-square combination of individual radius-related errors ($\Delta g_{R_1}$, $\Delta g_{R_2}$, $\Delta g_{R_3}$). Other sources of uncertainty—nuclear recoil, nuclear polarization, and nuclear model—are included identically for all isotope pairs.

A detailed analysis of the uncertainties reveals that the dominant contribution to the total error arises from FNS correction, primarily due to experimental uncertainties in the nuclear charge radii and model dependence. This contribution exceeds other sources, such as nuclear recoil and nuclear polarization.

Two methods were used to evaluate the impact of radius uncertainties: root-mean-square combination and conservative upper-bound estimation. Despite the methodological difference, both approaches confirm that the radii-related uncertainty is the important factor in establishing bounds on new physics.

These findings underscore the importance of improving nuclear radius measurements to enhance the sensitivity of $g$-factor–based tests of new physics. Furthermore, alternative strategies, such as the special differences method, aimed at reducing the FNS contribution, warrant further investigation.

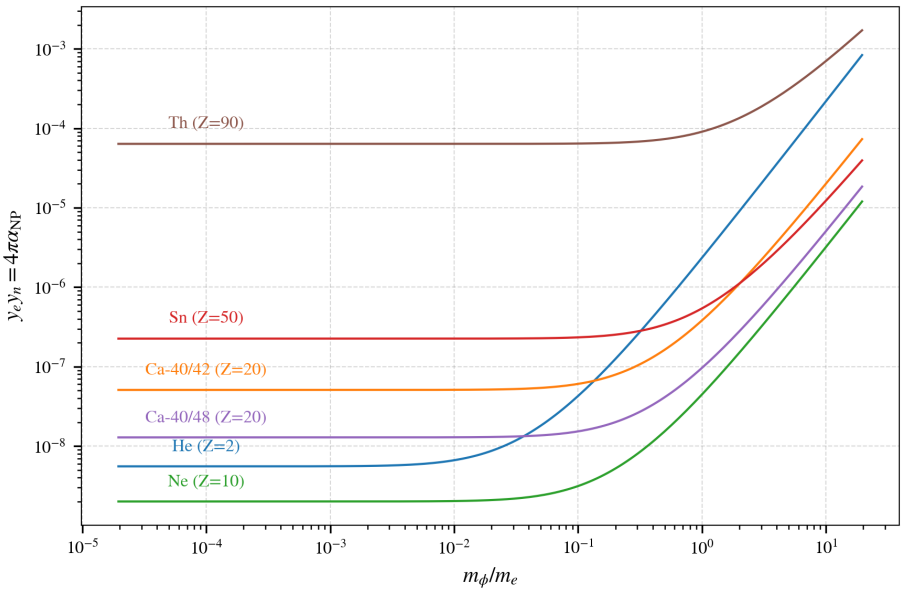


**Figure 3.** Same as Figure 2, but with nuclear radius uncertainties estimated via maximization approach (upper-bound error estimation). This conservative method takes the largest possible deviation in finite nuclear size correction due to radius errors, leading to less stringent constraints on $\alpha_{\rm NB}$. All other uncertainties remain identical to those in Figure 2.

## 6. Conclusions

In this work, we performed a detailed uncertainty analysis for the isotope shift of the bound-electron $g$ factor in hydrogen-like highly charged ions. All major quantum electrodynamics contributions were taken into account, including finite nuclear size, nuclear recoil, and nuclear polarization effects. For each of these contributions, we evaluated the associated uncertainties and identified their relative impact on the total error budget.

Our results demonstrate that the dominant and irreducible source of uncertainty stems from the finite nuclear size correction. Importantly, we found that the sensitivity of the isotope shift method does not increase with the nuclear charge $Z$ as might be intuitively expected; instead, it tends to decrease, primarily due to the growing impact of FNS uncertainties in heavy nuclei.

These findings emphasize the need for improved experimental determinations of nuclear radii and motivate the application of alternative strategies, such as the special differences method, which aim to suppress finite size contributions. The methodology developed in this work provides a robust basis for future refinement of theoretical models and more precise searches for new physics through $g$ factor measurements.

**Author Contributions:** Conceptualization and methodology: D.S.A., R.R.A., D.V.C., D.A.G., and A.V.V.; Calculations: D.S.A. and R.R.A.; Writing—original draft preparation (Section "Field shift"): D.S.A.; Writing—original draft preparation (Section "Corrections for mass shift. Nuclear recoil"): R.R.A.; Writing—review and editing: R.R.A. and D.V.C. All authors have read and agreed to the published version of the manuscript.

**Funding:** The work presented in Sections 2, 4, and 5 was supported by the Russian Science Foundation (Grant No. 24-72-10060). The work presented in Section 3 was supported by the Ministry of Science and Higher Education of the Russian Federation (Project FSER-2025–0012).

**Data Availability Statement:** The data presented in this study can be made available upon request.

**Acknowledgments:** We would like to thank Aleksei Malyshev for sharing his results on the higher-order nuclear recoil contribution with a finite nuclear size.

**Conflicts of Interest:** The authors declare no conflicts of interest. The funders had no role in the design of the study; in the collection, analyses, or interpretation of data; in the writing of the manuscript; or in the decision to publish the results.

## References


1. Aoyama, T.; Kinoshita, T.; Nio, M. Theory of the Anomalous Magnetic Moment of the Electron. *Atoms* **2019**, *7*, 28. [CrossRef]
2. Fan, X.; Myers, T.G.; Sukra, B.A.D.; Gabrielse, G. Measurement of the Electron Magnetic Moment. *Phys. Rev. Lett.* **2023**, *130*, 071801. [CrossRef]
3. Sturm, S.; Köhler, F.; Zatorski, J.; Wagner, A.; Harman, Z.; Werth, G.; Quint, W.; Keitel, C.H.; Blaum, K. High-precision measurement of the atomic mass of the electron. *Nature* **2014**, *506*, 467. [CrossRef]
4. Arapoglou, I.; Egl, A.; Höcker, M.; Sailer, T.; Tu, B.; Weigel, A.; Wolf, R.; Cakir, H.; Yerokhin, V.A.; Oreshkina, N.S.; et al. The g-factor of Boronlike Argon $^{40}Ar^{13+}$. *Phys. Rev. Lett.* **2019**, *122*, 253001. [CrossRef]
5. Glazov, D.A.; Köhler-Langes, F.; Volotka, A.V.; Blaum, K.; Heiße, F.; Plunien, G.; Quint, W.; Rau, S.; Shabaev, V.M.; Sturm, S.; et al. g Factor of Lithiumlike Silicon: New Challenge to Bound-State QED. *Phys. Rev. Lett.* **2019**, *123*, 173001. [CrossRef]
6. Micke, P.; Leopold, T.; King, S.A.; Benkler, E.; Spieß, L.; Schmöger, L.; Schwarz, M.; Crespo López-Urrutia, J.R.; Schmidt, P.O. Coherent Laser Spectroscopy of Highly Charged Ions Using Quantum Logic. *Nature* **2020**, *578*, 60–65. [CrossRef]
7. Köhler, F.; Blaum, K.; Block, M.; Chenmarev, S.; Eliseev, S.; Glazov, D.A.; Goncharov, M.; Hou, J.; Kracke, A.; Nesterenko, D.A.; et al. Isotope dependence of the Zeeman effect in lithium-like calcium. *Nat. Commun.* **2016**, *7*, 10246. [CrossRef]
8. Blaum, K.; Eliseev, S.; Sturm, S. High-Precision Mass Measurements and Their Impact on Fundamental Constants and Tests of the Standard Model. *Quantum Sci. Technol.* **2021**, *6*, 014002. [CrossRef]
9. Morgner, J.; Tu, B.; König, C.; Sailer, T.; Heiße, F.; Bekker, H.; Sikora, B.; Lyu, C.; Yerokhin, V.A.; Harman, Z.; et al. Stringent test of QED with hydrogen-like tin. *Nature* **2023**, *622*, 53–57. [CrossRef]
10. Morgner, J.; Tu, B.; Moretti, M.; König, C.M.; Heiße, F.; Sailer, T.; Yerokhin, V.A.; Sikora, B.; Oreshkina, N.S.; Harman, Z.; et al. *g* Factor of Boronlike Tin. *Phys. Rev. Lett.* **2025**, *134*, 123201. [CrossRef]
11. Sailer, T.; Debierre, V.; Harman, Z.; Heiße, F.; König, C.; Morgner, J.; Tu, B.; Volotka, A.V.; Keitel, C.H.; Blaum, K.; et al. Measurement of the bound-electron g-factor difference in coupled ions. *Nature* **2022**, *606*, 479–483. [CrossRef] [PubMed]
12. Glazov, D.; Zinenko, D.; Agababaev, V.; Moshkin, A.; Tryapitsyna, E.; Volchkova, A.; Volotka, A. g Factor of Few-Electron Highly Charged Ions. *Atoms* **2023**, *11*, 119. [CrossRef]
13. Shabaev, V.M.; Glazov, D.A.; Plunien, G.; Volotka, A.V. Theory of bound-electron g factor in highly charged ions. *J. Phys. Chem. Ref. Data* **2015**, *44*, 031205. [CrossRef]
14. Volotka, A.V.; Plunien, G. Nuclear Polarization Study: New Frontiers for Tests of QED in Heavy Highly Charged Ions. *Phys. Rev. Lett.* **2014**, *113*, 023002. [CrossRef]
15. Mohr, P.J.; Plunien, G.; Soff, G. QED corrections in heavy atoms. *Phys. Rep.* **1998**, *293*, 227–369. [CrossRef]
16. Nefiodov, A.V.; Plunien, G.; Soff, G. Nuclear-polarization correction to the bound-electron g factor in heavy hydrogenlike ions. *Phys. Rev. Lett.* **2002**, *89*, 081802. [CrossRef]
17. Rinker, G.A.; Speth, J. Nuclear polarization in muonic atoms. *Nucl. Phys. A* **1978**, *306*, 397–405. [CrossRef]
18. Kozhedub, Y.S.; Andreev, O.V.; Shabaev, V.M.; Tupitsyn, I.I.; Brandau, C.; Kozhuharov, C.; Plunien, G.; Stöhlker, T. Nuclear Deformation Effect on the Binding Energies in Heavy Ions. *Phys. Rev. A* **2008**, *77*, 032501. [CrossRef]
19. Sun, Z.; Valuev, I.A.; Oreshkina, N.S. Nuclear Deformation Effects in the Spectra of Highly Charged Ions. *Phys. Rev. Res.* **2024**, *6*, 023327. [CrossRef]
20. Glazov, D.A.; Shabaev, V.M. Finite nuclear size correction to the bound-electron g factor in a hydrogenlike atom. *Phys. Lett. A* **2002**, *297*, 408–411. [CrossRef]
21. Zwicky, F. Die Rotverschiebung von extragalaktischen Nebeln. *Helv. Phys. Acta* **1933**, *6*, 110–127. [CrossRef]
22. Graham, P.W.; Kaplan, D.E.; Rajendran, S. Cosmological Relaxation of the Electroweak Scale. *Phys. Rev. Lett.* **2015**, *115*, 221801. [CrossRef] [PubMed]
23. Sakharov, A.D. Violation of CP invariance, C asymmetry, and baryon asymmetry of the universe. *JETP Lett.* **1967**, *5*, 32–35. [CrossRef].
24. Debierre, V.; Keitel, C.H.; Harman, Z. Fifth-force search with the bound-electron g factor. *Phys. Lett. B* **2020**, *807*, 135527. [CrossRef]
25. Debierre, V.; Oreshkina, N.S.; Valuev, I.A.; Harman, Z.; Keitel, C.H. Testing standard-model extensions with isotope shifts in few-electron ions. *Phys. Rev. A* **2022**, *106*, 062801. [CrossRef]
26. Shabaev, V.M.; Glazov, D.A.; Malyshev, A.V.; Tupitsyn, I.I. Recoil Effect on the *g* Factor of Li-Like Ions. *Phys. Rev. Lett.* **2017**, *119*, 263001. [CrossRef]
27. Shabaev, V.M.; Glazov, D.A.; Malyshev, A.V.; Tupitsyn, I.I. Nuclear recoil effect on the *g* factor of highly charged Li-like ions. *Phys. Rev. A* **2018**, *98*, 032512. [CrossRef]

28. Shabaev, V.M.; Yerokhin, V.A. Recoil correction to the bound-electron g factor in H-like atoms to all orders in $\alpha Z$. *Phys. Rev. Lett.* **2002**, *88*, 091801. [CrossRef]
29. Arcadi, G.; Djouadi, A.; Raidal, M. Dark Matter through the Higgs portal. *Phys. Rep.* **2020**, *842*, 1–180. [CrossRef]
30. Shabaev, V.M.; Tupitsyn, I.I.; Yerokhin, V.A.; Plunien, G.; Soff, G. Dual Kinetic Balance Approach to Basis-Set Expansions for the Dirac Equation. *Phys. Rev. Lett.* **2004**, *93*, 130405. [CrossRef]
31. Angeli, I.; Marinova, K.P. Table of experimental nuclear ground state charge radii: An update. *At. Data Nucl. Data Tables* **2013**, *99*, 69–95. [CrossRef]
32. Fricke, G.; Heilig, K. *Nuclear Charge Radii*; Springer: Berlin/Heidelberg, Germany, 2004; pp. 18–350. [CrossRef]
33. Mårtensson-Pendrill, A.M.; Ynnerman, A.; Warston, H.; Vermeeren, L.; Silverans, R.E.; Klein, A.; Neugart, R.; Schulz, C.; Lievens, P. The ISOLDE Collaboration. Isotope Shifts and Nuclear-Charge Radii in Singly Ionized $^{40-48}$Ca. *Phys. Rev. A* **1992**, *45*, 4675–4681. [CrossRef] [PubMed]
34. De Vries, H.; De Jager, C.W.; De Vries, C. Nuclear Charge-Density-Distribution Parameters from Elastic Electron Scattering. *At. Data Nucl. Data Tables* **1987**, *36*, 495–536. [CrossRef]
35. Pieper, S.C.; Wiringa, R.B. Quantum Monte Carlo Calculations of Light Nuclei. *Annu. Rev. Nucl. Part. Sci.* **2001**, *51*, 53–90. [CrossRef]
36. Friar, J.L.; Schwieger, J.; Faessler, A.; Kosmas, T.S. Nuclear Size Effects in Light Atoms. *Phys. Rev. C* **1997**, *56*, 2830–2835. [CrossRef]
37. Johnson, W.R.; Blundell, S.A.; Sapirstein, J. Finite basis sets for the Dirac equation constructed from B splines. *Phys. Rev. A* **1988**, *37*, 307–315. [CrossRef]
38. Shabaev, V.M. QED theory of the nuclear recoil effect on the atomic g factor. *Phys. Rev. A* **2001**, *64*, 052104. [CrossRef]
39. Grotch, H.; Hegstrom, R.A. Hydrogenic Atoms in a Magnetic Field. *Phys. Rev. A* **1971**, *4*, 59–69. [CrossRef]
40. Pachucki, K. Nuclear mass correction to the magnetic interaction of atomic systems. *Phys. Rev. A* **2008**, *78*, 012504. [CrossRef]
41. Close, F.E.; Osborn, H. Relativistic extension of the electromagnetic current for composite systems. *Phys. Lett. B* **1971**, *34*, 400–404. [CrossRef]
42. Eides, M.I.; Grotch, H. Gyromagnetic Ratios of Bound Particles. *Ann. Phys.* **1997**, *260*, 191–200. [CrossRef]
43. Eides, M.I.; Martin, T.J.S. Universal Binding and Recoil Corrections to Bound State g Factors in Hydrogenlike Ions. *Phys. Rev. Lett.* **2010**, *105*, 100402. [CrossRef] [PubMed]